HHS Public Access

Author manuscript

Cancer Res. Author manuscript; available in PMC 2023 March 10.

Published in final edited form as:

Cancer Res. 2021 February 01; 81(3): 698–712. doi:10.1158/0008-5472.CAN-20-2066.

Axl and Mertk receptors cooperate to promote breast cancer progression by combined oncogenic signaling and evasion of host anti-tumor immunity

Viralkumar Davra[1], **Sushil Kumar**[1,2,3], **Ke Geng**[1], **David Calianese**[1], **Dhriti Mehta**[1], **Varsha Gadiyar**[1], **Canan Kasikara**[1,4], **Kevin C. Lahey**[1], **Yun-juan Chang**[5], **Michael Wichroski**[6], **Chan Gao**[6], **Mariana S. De Lorenzo**[7], **Sergei V. Kotenko**[1], **Tessa Bergsbaken**[8], **Pankaj K. Mishra**[8], **William C. Gause**[8], **Michael Quigley**[6], **Thomas E. Spires**[6], **Raymond B. Birge**[1,*]

[1]Department of Microbiology, Biochemistry and Molecular Genetics, Cancer Center, Rutgers-New Jersey Medical School, 205 South Orange Ave, Newark, NJ, 07103

[2]Present address: Department of Cancer Immunology and Virology, Dana-Farber Cancer Institute, Boston, MA

[3]Present address: Department of Microbiology and Immunobiology, Harvard Medical School, Boston, MA, 02115

[4]Present address: Columbia Presbyterian Medical Center, College of Physicians & Surgeons of Columbia University. 630 West 168th street, PH9-405, New York, NY 10032

[5]Office of Advanced Research Computing, Rutgers- New Jersey Medical School, 185 South Orange Ave, Newark, NJ, 07103

[6]Bristol Myers Squibb. Lawrenceville, New Jersey

[7]Department of Cell Biology, New Jersey Medical School, 185 South Orange Ave, Newark, NJ, 07103

[8]Center for Immunity and Inflammation. Rutgers, Biomedical and Health Sciences, 205 South Orange Ave, Newark, NJ, 07103

Abstract

Despite the promising clinical benefit of targeted and immune checkpoint blocking therapeutics, current strategies have limited success in breast cancer, indicating that additional inhibitory pathways are required to complement existing therapeutics. TAM receptors (Tyro-3, Axl,

[*]**Corresponding Author:** Raymond B. Birge, birgera@njms.rutgers.edu. Tel.: 973-972-4497; Fax: 973-972-5594. Rutgers- New Jersey Medical School, Cancer Center, 205 South Orange Ave, Newark, NJ, 07103.

Authors' contributions

Viralkumar Davra designed the study, performed the experiments, analyzed the data and wrote the manuscript. Sushil Kumar, Ke Geng, Samuel Desind, David Calianese, Dhriti Mehta, Varsha Gadiyar, Canan Kasikara and Panjkaj K. Mishra performed the experiments and analyzed the results. Thomas Spires, Michael Wichroski, Chan Gao, and Michael Quigley provided Anti-Mertk and Anti-PD-1 mAb and helped in preparation of manuscript and interpretation of tumor data. Tessa Bergsbaken, Sergei Kotenko, Mariana S. De Lorenzo, and Willian C. Gause provided technical support and reagents, and helped data interpretation. Raymond B. Birge conceived and coordinated the study, helped in design of experiments and wrote the paper. All authors reviewed the results and approved the final version of the manuscript.

Disclosure of potential conflicts of interest: No potential conflicts of interest were disclosed by the authors. Thomas Spires, Michael Quigley, Chan Gao and Michael Wichroski are employees of Bristol-Myers Squibb.

and Mertk) are often correlated with poor prognosis due to their capacities to sustain an immunosuppressive environment. Here we ablate Axl on tumor cells using CRISPR/Cas9 gene editing, and by targeting Mertk in the tumor microenvironment, we observe distinct functions of TAM as oncogenic kinases as well as inhibitory immune receptors. Depletion of Axl suppressed cell intrinsic oncogenic properties, decreased tumor growth, reduced the incidence of lung metastasis and increased overall survival of mice when injected into mammary fatpad of syngeneic mice, and demonstrated synergy when combined with anti-PD1 therapy. Blockade of Mertk function on macrophages decreased efferocytosis, altered the cytokine milieu, and resulted in suppressed macrophage gene expression patterns. Mertk KO mice or treatment with anti-Mertk neutralizing mAb also altered the cellular immune profile, resulting in a more inflamed tumor environment with enhanced T cell infiltration into tumors and T cell-mediated cytotoxicity. The anti-tumor activity from Mertk inhibition was abrogated by depletion of cytotoxic CD8α T cells by using anti-CD8α mAb or by transplantation of tumor cells into B6.CB17-Prkdc SCID mice. Our data indicate that targeting Axl expressed on tumor cells and Mertk in the tumor microenvironment are predicted to have a combinatorial benefit to enhance current immunotherapies and that Axl and Mertk have distinct functional activities that impair host anti-tumor response.

Keywords

TAM receptor; Immunotherapy; Breast Cancer; Immune evasion; Metastasis

Introduction

In recent years, immunotherapies have emerged widely as promising therapeutic regimens, by blocking immune checkpoint molecules such as, PD-1, PD-L1 or CTLA-4, which are known to suppress host anti-tumor immunity in the tumor microenvironment (TME). However, the response rate of immunotherapy in solid tumors remains variable from 10–30%, primarily due to adaptive immune suppressive signals that exist in the tumor milieu [1,2]. We and others have proposed that constitutively elevated and externalized phosphatidylserine (PS) as a result of the high apoptotic indexes of solid tumors and the metabolically stressed tumor microenvironment (TME) represents a locally immunosuppressive modality that impinges on host anti-tumor immunogenic signals [3] [4]. Such increased local concentration of PS and PS-positive tumor mass has been often associated with poorer survival outcomes and tumor progression [5,6]. The externalization of PS, and subsequent interactions with PS receptors such as Tyro3, Axl, and Mertk (abbreviated TAM) receptors has been shown to have important immunological consequences [7] [8].

Functionally, TAMs are broadly expressed on several cell types in the TME, including tumor cells, macrophages, dendritic cells, myeloid-derived suppressor cells, NK cells, and more recently have been reported on T cells [9], where they interact with PS on the surface of dying apoptotic cells through the bridging molecules, Growth Arrest Gene Factor 6 (Gas6) [10] and Protein S (Pros1)) [11]. By mechanisms that are still not completely understood, Mertk on professional phagocytes regulates the suppression of transcription factors, such

as STAT1 [12], NF-κB [13], and pro-inflammatory cytokines such as TNF-α [14], and IFN-γ [15], while inducing the expression of anti-inflammatory and tolerogenic cytokines such as IL-10, IL-4, and TGF-β [16]. In normal tissues, the aforementioned responses are important for tissue homeostasis and the timely resolution of acute inflammation and tissue repair [17]. This homeostatic function of Mertk is supported by both genetic and pharmacological approaches which show that loss of Mertk function can lead to chronic inflammatory diseases, including a lupus-like disease in older mice [18,19], atherosclerosis in hypercholesterolemic mice [20], and NASH in high-fat diet fed mice [21].

In contrast to the homeostatic and tolerogenic functions of Mertk to prevent chronic inflammation and autoimmunity, in cancer models, aforementioned immunomodulatory responses regulated by Mertk (and likely other TAMs) represent pathophysiological events that suppress or inhibit effective host anti-tumor immune responses [8]. Cook and colleagues showed that in a syngeneic model of breast cancer, transplantation of Mertk$^{-/-}$ bone marrow cells into lethally irradiated tumor-bearing mice suppressed tumor growth compared to transplantation of WT bone marrow, suggesting that host Mertk function is permissive for tumor progression [22]. Mertk activation on tumor macrophages has also been shown to promote tumor growth and recurrence following radiation therapy, whereby the loss of Mertk (Mertk$^{-/-}$ mice) plus focal radiation therapy is sufficient to prevent recurrence and promote survival [23] [24]. Recently Zhou et. al showed that antibody-mediated Mertk blockade enhances immunogenicity and synergizes with ant-PD1 mAb by inducing a tumor cGas-Sting-dependent type I IFN response [25].

TAMs also have direct oncogenic fucntions when up-regulated and overexpressed on cancer cells [7]. Overexpression or constitutive activation of Axl on tumor cells has been linked with epithelial to mesenchymal transition (EMT) [26–28] and cancer stemness; which are associated with tumor invasion, metastasis, chemoresistance, and disease progression [29,30]. In the case for Axl, overexpression of Axl in mammary epithelial cells resulted in decreased E-Cadherin and in increase in mesenchymal markers N-Cadherin, Vimentin, and Snail [31]. Additionally, treatment of TNBC cells with Gas6 results in increased expression of EMT-associated genes including Snail and Slug [32]. TAM-directed epithelial efferocytosis been shown to induce expression of the immune checkpoint blockade inhibitor PD-L1, providing another mode of suppressive immune modulation in the TME that could negatively impact T cell function [33].

Previously, using an immune-competent syngeneic murine model of triple negative breast cancer in immune competent mice, we reported that a pan-TAM tyrosine kinase inhibitor (BMS-777607) which has potent low nanomolar activity against all three TAMs (Tyro3, Axl, and Mertk) promoted both anti-tumor and anti-metastatic activity, and induced a significant host anti-tumor responses that acted synergistically with anti-PD1 blockade [34]. The objective of the present study was to dissociate the differential functions of TAMs, particularly Axl and Mertk, expressed on tumor cells versus on the in the host immune cells. By ablating Axl on tumor cells via CRISPR/Cas9 gene editing, and by targeting Mertk in the tumor microenvironment by using Mertk knockout mice or by an anti-Mertk neutralizing mAb, we observed distinct functions of TAMs as oncogenic kinases as well as inhibitory immune receptors. Overall, this study supports a synergistic biology based on the differential

expression of Axl and Mertk in the TME, and that both receptors cooperate to promote oncogenesis and immune escape by dinstinct mechansims. In addition, the study emphasizes the continued development of TAM inhibitors in immuno-oncology.

Materials and Methods

Cell culture and generation of Axl receptor KO in murine breast cancer cell lines

The murine triple negative breast cancer cell lines 4T1-Luc-GFP (Perkin-Elmer) and E0771 (CH3 Biosystems (CH3 Biosystems LLC) were maintained in RPMI-1640 medium (Sigma-Aldrich) supplemented with 10% v/v fetal bovine serum (FBS) (Atlanta biologics), 100 IU/ml penicillin and 100 μg/ml streptomycin (Sigma-Aldrich). Cells were grown at 37°C in a humidified incubator containing 5% CO_2. Two individual guide RNAs targeting the Axl (GCGCCAACCACCAGGCCAGCGG, GAGGCTGGCAGCCCGTTTGTGG) were synthesized and cloned into all-in-one plasmid vector (U6-gRNA/CMV/Cas9-RFP) from Sigma-Aldrich. The vectors containing guide RNAs were transfected individually, sorted for RFP-positive single cells by flow cytometry. Single cell clones were grown and screened by Western blotting for Axl receptor KO followed by confirmation using flow cytometry. Stable re-expression of Axl receptor in the 4T1 and E0771 Axl KO cells were induced by retroviral infection of host BOSC23 cells co-transfected with pCL-Eco, pMD2.G and pMSCV-mAxl followed by selection with puromycin for two weeks. After thawing, cells were used for up to 8–10 passages and their authenticities were checked by Short Tandem Repeat (STR) analysis according to manufacturer's protocol (GenePrint 10 System, Promega). Cells were routinely checked for mycoplasma contamination.

Protein Isolation and Western blot analysis

Whole cell lysates of cells were prepared in HNTG buffer (20mM HEPES, pH 7.5, 150mM NaCl, 10% glycerol) supplemented with 1% Triton X-100, 1mM PMSF, 1mM sodium orthovanadate, 10mM sodium molybdate, 1mM EDTA, 10mM sodium fluoride and 1% protease inhibitor cocktail. Western blot analyses were performed using antibodies as follows: anti-Axl (SCBT), anti-phospho-Axl (Sigma), anti-phospho-Akt (Ser473) (Cell Signaling, 193H12), anti-Vimentin (Cell Signaling, D21H3), anti-E-Cadherin (Cell Signaling, 24E10), anti-β-Catenin (Cell Signaling, D10A8), anti-Zeb-1 (Cell Signaling, D80D3), anti-Zo-1 (Cell Signaling, D7D12), anti-β-Actin (Cell Signaling, MAB374), and anti-phospho-STAT1 (BD Bioscience, 612233) antibodies.

Tumorsphere formation assay

To assess the tumorsphere formation efficiency, 1×10^3 4T1-WT and Axl KO cells were seeded as triplicate in Ultra-Low attachment 24 well plate (Corning Costar). The cells were allowed to make tumorsphere for 10 days and subsequently, the number and size of tumorspheres were analyzed. The typical tumorsphere is >100 μm in diameter and round in shape.

Wound healing assay

4T1-WT and Axl KO cells were seeded in 6 well plates for 18 hrs followed by starvation in RPMI medium containing 0.5% FBS (Starvation medium) for 8 hrs. Subsequently, cells

were washed twice with starvation medium and supplied with complete RPMI medium. Using 200 μl sterile pipette tip a scratch was created under sterile conditions and migration of cells into the gap generated was observed.

Real-time cell migration and invasion assay using xCELLigence system

Real-time cell migration and cell invasion assay was performed using xCELLigence RTCA system. Briefly, 4T1 WT and Axl KO cells were serum starved for 8 hrs in RPMI medium containing 0.5% FBS (Starvation medium). RPMI medium containing 10% FBS was added as chemoattractant in the lower chamber and 50 μl of starvation medium was added in the top chamber of CIM-16 plates and plates were kept for equilibration for 1 hr. After 1 hr, 40000 - WT and Axl KO cells suspended in 100 μl starvation medium with and without Gas6 were added in triplicates in the upper chamber wells and changes in cell index (CI) depicting cellular migration, were assessed every 10 mins for mentioned time periods. For cell invasion assay, an additional 10% matrigel plug was used in the upper chamber.

In vivo mouse experiments

The mouse isotype control, anti-PD-1 (4H2) and anti-Mertk (16B9) mAbs (all kindly gifted by Bristol Myers Squibb) were used as treatment regimens. For *in vivo* studies, 7 weeks old, female BALB/c, c57BL/6 and B6.CB17-Prkdc SCID mice were obtained from Jackson laboratory, whereas Mertk$^{(-/-)}$ mice were bred at Rutgers University's animal facility. The mice were housed in pathogen-free facility, maintained under a strict 12 hr light cycle, and been given regular chow diet. For tumor cell inoculation, 50,000 4T1-Luc-GFP or E0771-WT, Axl KO and Axl Re-Exp cells were re-suspended in RPMI-1640 complete medium containing Matrigel (50 % v/v) (Corning) and injected into the 9/10 mammary fat pad of the BALB/c and c57BL/6 mice (n=8/group) respectively. Similar to above approach, 50,000 E0771- WT, Axl KO cells were injected in the age-matched 7 weeks old Mertk$^{(-/-)}$ and B6.CB17-Prkdc SCID female mice. The chimeric anti-PD-1 (4H2) and anti-Mertk mAb were used as treatment regimens. The anti-mouse IgG1 isotype antibody control (15 mg/kg) as vehicle control, anti-Mertk ab (10 mg/kg) alone, anti-PD-1(5 mg/kg) alone or in combination were injected intraperitoneally on days 6, 9, 12, and 15. Doses were selected through preliminary maximum tolerated dose (MTD) studies performed at the Bristol Myers Squibb. To deplete cytotoxic CD8α T-cells, mice were injected intraperitoneally with 200 μg anti-CD8α (clone 2.43; BioXCell) a day before tumor cell injection and followed by every 3 days until the end of study. The dose regimen for Anti-CD8-α Ab was selected based upon several studies suggesting almost complete depletion of cytotoxic CD8+ T-cell as this dosage was observed [35]. Tumor growth and body weights were assessed twice a week by caliper measurement of tumor diameter in the longest dimension (L) and at right angles to that axis (W). Tumor volumes were estimated using the formula, $L \times W \times W \times \pi/6$. To represent consistencies between Axl KO, Mertk KO, and pharmacologic anti-Mertk inhibition with or without immunotherapy, tumor volume were normalized to the final day tumor volume of control mice.Toxicity and weight loss were not encountered in the studies. When metastases were found, the organ was removed and fixed for quantification and histopathology analysis. To determine lung metastasis, lungs were isolated and washed with PBS and incubated in Bouin solution for 48 hrs. The lung metastatic nodules were counted using stereomicroscope by two investigators separately. Long rank test has been

performed and values have been included in the respective KM plots. Mouse experiments were performed in accordance with the guidelines and under the approval from Institutional Animal Care and Use Committee at the Rutgers University, NJMS.

NanoString immune-profiling analysis

For Nanostring analysis, total RNA was isolated from 4 primary snap frozen tumors from each treatment group (Isotype, Axl KO, Anti-Mertk mAb and anti-PD-1 alone and Axl KO and Anti-Mertk mAb with anti-PD-1 combination) by using RNeasy Plus total RNA Isolation kit (QIAGEN). All the RNA samples have passed quality control (assessed by OD 260/280) and were subjected to analysis by nCounter murine PanCancer Immune Profiling Panel according to the manufacturer's protocol at NYU Genomic Center (NanoString Technologies). Normalization of raw data was performed using the nSolver 3.0 analysis software (NanoString Technologies). The mean of each gene expression (represented in log2) for each treatment group was calculated and the statistical analysis and graphics was performed using Graphpad Prism software for statistical analysis. Further advanced immune-profiling analysis was performed using nSolver 3.0 analysis software with nCounter advanced analysis package (NanoString Technologies) with identified immune cell types.

Bone marrow derived and peritoneal macrophage culture

The tibias and femurs were collected from 6–8-week-old mice and were crushed using mortar and pestle with 5 mL DMEM/F12K medium containing 10% HI FBS and 1% Pen/Strep (BMDM medium). The bone marrow cells were pipetted up and down to bring the cells into single-cell suspension followed by centrifugation at the 1500 rpm for 5 mins at 4°C and red blood cells were lysed with RBC lysis buffer for 5 mins at room temperature. The cells were passed through a 70μm cell strainer followed by washing the strainer with 10 mL BMDM medium and centrifugation at the 1500 rpm for 5 mins at 4°C. The cells were re-suspended in the BMDM medium containing 20% L929 Conditioned medium (L929 medium). The bone marrow cells were counted, and 3×10^6 cells in 20 ml L929 medium were plated 15 cm plate. Fresh 20 ml L929 medium was added on day 3. On Day 7, macrophages were washed once with PBS and split by scrapping the cells as per the experimental requirement in BMDM medium. For Mertk receptor induction, BMDMs were treated with 0.1 μM dexamethasone for 24 hrs. For peritoneal macrophage (PEC) isolation, 1 ml PBS was injected intraperitoneally in mice 48 hrs before macrophage isolation. The peritoneal exudate was collected by washing the peritoneal cavity twice with RPMI medium containing 10% HI FBS and 1% Pen/Strep (PEC medium) and macrophages were purified using biotinylated anti-mouse F4/80 antibody (Biolegend, BM8) followed by anti-biotin micro bids (Miltenyi Biotec). More than 95% purity was obtained when analyzed by anti-mouse CD11b (ebioscience, M1/70, PerCP-Cy5.5) and anti-mouse F4/80 (Biolegend, BM8, APC) staining using flow cytometry.

Efferocytosis Assay

The differentiated BMDMs were plated on 6-well plate starved in DMEM/F12K medium with 0.5% FBS with or without dexamethasone for 18 hrs. The apoptotic cells were prepared from CEM, human T lymphoblast, cells by UV irradiation (50000 μJ/cm^2) using CL-1000 UV cross linker. The irradiated CEM cells were incubated for 5 hrs in RPMI medium only

in the 37 C incubator followed by staining with 100 ng/ml pHrodo-SE (Invitrogen) for 30 min. The labeled cells were then washed twice in PBS containing 1% BSA and 1 mM EDTA and once with DMEM/F12 medium only. The apoptotic cells were then incubated for 10 min with Gas6 supernatant. The apoptotic cells-Gas6 mixture was then added to macrophages at the ratio 3:1 (apoptotic cells: macrophage) and incubated for 45 min at 37°C. The macrophages were washed twice with PBS and then scraped using cell scraper. Efferocytosis was assessed by analyzing CD11b, F4/80 and pHrodo positive macrophages using flow cytometry.

For *ex vivo* efferocytosis, peritoneal macrophages were incubated with various concentrations of either the anti-Mertk or Isotype control antibodies. Thymocytes were collected and treated with camptothecin for 2 hours to induce apoptosis, washed and then treated with pHrodo for 30 minutes at room temperature and washed. Labeled thymoctes (5×10^5) were then added to the peritoneal macrophages and allowed to incubate for 1 hour. Cells were then harevsted and stained with CD11b and F4/80 antibodies (BioLegend) run on a BD FACSCanto. The proportion of pHrodo positive CD11b+F4/80+ cells was then determined and IC_{50} determinations made using XLFit. For *in vivo* efferocytosis, 1 ml PBS was injected intraperitoneally in WT and Mertk$^{(-/-)}$ mice 48 hrs before apoptotic cells injection. Apoptotic cells were prepared and stained as mentioned earlier and 1 X 10^7 pHrodo stained apoptotic cells were injected in the intraperitoneal cavity for 1 hr. Peritoneal exudate was collected and macrophage efferocytosis was analyzed by flow cytometry.

RNASeq Analysis

Following *in vivo* efferocytosis, CD11b+F4/80+ and CD11b+F4/80+pHrodo+ macropaheges from untreated and treated mice were flow sorted and total cellular RNA was extracted and analyzed for integrity and samples with RNA integrity number (RIN) >9.0 were used for subsequent processing. Total RNA was subjected to two rounds of poly(A) selection using oligo-d(T)25 magnetic beads. A single-read (strand specific) cDNA library was prepared following the Illumina TrueSeq small RNA protocol for strand-specific RNA-seq with minor modifications. Briefly, poly(A) + RNA was fragmented in an alkaline buffer (NaHCO3 at pH 9.3) for 2 min at 94 °C followed by dephosphorylation with recombinant shrimp alkaline phosphatase and phosphorylation with T4 poly- nucleotide kinase. After addition of 3′ adapter (5′ adeny- lated) and 5′ adapter using truncated T4 RNA ligase II and T4 RNA ligase I, respectively, RNA was reverse- transcribed using 3′ adapter-specific primer. cDNA was then amplified by PCR for 15 cycles with a universal forward primer and a reverse primer with bar code. The cDNA libraries were purified using AmpureXP beads and quantified on an Agilent Bioanalyzer (Additional file 1). Sequencing was done on NextSeq 500 Illumina with 1×75 configuration. Raw reads were quality trimmed using Trimmomatic-0.39 with leading and trailing Q score 30, minimum length 30 bp. The cleaned reads were mapped to *Mus musculus* genome GRCm38 using HISAT2 (v.2.1.0). The reference genome sequence and annotation files were downloaded from ENSEMBLE, release.97 (Mus_musculus.GRCm38.97.fa, and Mus_musculus.GRCm38.97.gtf). The aligned read counts were obtained using htseq-count as part of the package HTSeq-0.6.1. The bioconductor package edgeR_3.18.1 with limma_3.32.10 was used to perform the differential gene expression analysis,

under R environment, R version 3.5.0. Reads were also mapped to Human genome reference (downloaded from ENSEMBLE, release 97, Homo_sapiens.GRCh38.97.fa and Homo_sapiens.GRCh38.97.gtf), using the same method to evaluate the potential human cell contamination.

Statistical analysis.

All *in vitro* and *in vivo* experiments were repeated at least three time. All differences between groups in all in vivo experiments were examined for statistical significance using a two- tailed Student's t-test and one-way ANOVA to compare multiple groups. GraphPad Prism software was used to perform statistical analysis. $P < 0.05$ was considered significant.

Results

Axl receptor deletion in breast cancer cells reduces oncogenic and tumorigenic potential.

Previously, we reported that a pan-TAM tyrosine kinase inhibitor (BMS-777607), which concomitantly targets Tyro3, Axl, and Mertk with low nanomolar affinity, has anti-tumor as well anti-metastatic effects, and increases host anti-tumor immunity in an orthotopic breast cancer model when combined with anti-PD1 blockade [34]. Here, in an attempt to better understand the role of Axl on tumor cells as compared to Mertk, which is predominantly expressed in the TME on myeloid-derived cells and tumor-associated macrophages, we took a dual approach. First, we generated Axl receptor deficient 4T1 and E0771 tumor cell lines by CRISPR/Cas9 gene editing, and second, we extrinsically inhibited Mertk (employing either $Mertk^{-/-}$ mice or a pharmacological anti-Mertk neutralizing mAb to block Mertk) in the TME.

As shown in Fig 1a-b, depletion of Axl receptor in the 4T1 or E0771 murine breast cancer cell lines were confirmed by Western blotting (Fig. 1a) and flow cytometry (Fig. 1b). To rule out off-target effects in subsequent *in vivo* studies, stable re-expression of Axl was achieved by ectopic gene delivery in the E0771 Axl knockout (Axl KO) cells. When wildtype (WT), Axl KO, and Axl re-expressed (Axl Re-Exp) cells were treated with Gas6 (a pan-TAM ligand), p-Akt (pSer473) was undetectable in the Axl KO cells, particularly in the E0771 cells, suggesting, Axl is the major Gas6 activated signaling receptor in E0771 cells but to a lesser extent in the 4T1 cells (Fig. 1c, S1a,b). Conversely, downstream signaling and AKT phosphorylation was restored in the Axl Re-Exp cells, following treatment with Gas6 (Fig. 1c).

To examine oncogenic potentials of Axl, we examined effects of the Axl deficient 4T1 cell, which has been previously shown to be a model of epithelial to mesenchymal transition (EMT) and spontaneous lung metastasis in immune-competent BALB/c mice [36]. As shown in Fig. 1d, when WT or Axl KO cells were seeded in ultralow attachment plates, which favors adherent cells to form tumorspheres, the native 4T1- WT cells showed larger sized and increased numbers of tumorspheres relative to the 4T1 Axl KO cells, indicating a direct role for Axl on the tumorigenic potential and stem-like properties of the tumor cells. The rate of cell proliferation in the Axl KO cells was also decreased as compared to WT cells (Fig. 1e), when analyzed by MTT assay. Similarly, Axl KO cells showed reduced cell

migration when analyzed by wound healing assays (Fig. 1f, S1c), as well as a quantitative reduction in cell migration (Fig. 1g) and cell invasion (Fig. 1h) using RTCA xCELLigence real-time assays. Similar to phosphorylation of Akt, we also observed increase in cell migration and invasion in WT cells in the presence of Gas6, however, no effect of ligand was observed in the Axl KO cells (Fig 1g). Axl KO cells also showed a virtual loss of the mesenchymal marker Vimentin, decreased Zeb-1, and increased expression of epithelial markers, E-Cadherin and β-catenin, collectively indicating a mesenchymal to epithelial transition phenotype in the Axl KO cells (Fig. 1i, S1d-e). Axl re-expression also stabilized the expression of Vimentin (S1d), and produced a more mesenchymal like morphology (S1f).

By using triple negative breast cancer 4T1 and E0771 models, we explored the tumorigenic and immunogenic properties of Axl *in vivo*. Fig. 2 shows results when either 4T1 and E0771- WT, Axl KO and Axl Re-Exp cells were orthotopically transplanted into the mammary fat pad of BALB/c or c57BL/6 female mice respectively. In both the breast cancer models, Axl ablation led to diminished tumor growth (Fig. 2a, d), extended overall survival in mice (Fig. 2b, e) and reduced the number of lung metastasis (Fig. 2c, f), as compared to WT cells. When 4T1 or E0771 - Axl Re-Exp cells were implanted in mouse mammary fat pad, the effects of Axl KO on the tumor growth were reversed, suggesting a direct effect of Axl receptor on the observed tumor growth profiles.

Further, to examine whether Axl depletion overcomes resistance to anti-PD1 immunotherapy, mice bearing WT or Axl KO tumors were administered either isotype control or anti-PD1 mAb. Mice treated with anti-PD1 monotherapy mAb, similar to the Axl KO tumor-bearing mice, showed partial anti-tumor efficacy (approximately 50% total decreased in tumor growth in each case) (Fig. 2g, S2a,b). However, Axl KO and anti-PD1 mAb combination showed additive anti-tumor effect, whereby 7 out of 8 mice were rendered tumor free, with increased overall tumor free survival relative to either Axl KO or anti-PD1 mAb monotherapy (Fig. 2h). Additionally, when analyzed for splenomegaly, a measure of extramedullary hematopoiesis and putative bone marrow metastasis, Axl KO tumor bearing mice treated with anti-PD1 mAb suppressed splenomegaly, as shown by spleen weight (Fig. 2i) and spleen length (Fig. S2c), as compared to isotype control. No difference in the total body weight was noted among the mice in different treatment groups (Fig. S2d).

Whole-body genetic ablation of Mertk (Mertk$^{(-/-)}$) alters tumor growth and potentiates anti-PD1 mAb therapeutics.

To explore the anti-tumor role of host-expressed Mertk, E0771 WT cells were orthotopically transplanted into c57BL/6 WT (Mertk$^{+/+}$) or whole-body Mertk KO (Mertk$^{-/-}$) mice. The tumor growth was significantly decreased (Fig. 3a, S3a,b) and overall survival was improved in the Mertk$^{-/-}$ mice as compared to Mertk$^{+/+}$ mice (Fig. 3b). Notably, anti-PD1 mAb treatment in the context of the Mertk$^{(-/-)}$ tumor-bearing mice, showed near complete eradication of tumors and provided long-term tumor-free survival benefits. In addition, subsequent tumor re-inoculation on indicated days, d42 (0.1×10^6) and d80 (0.2×10^6), offered anti-tumor protection against subsequent tumor growth, suggesting that Mertk$^{-/-}$ tumor-bearing mice treated with anti-PD1 checkpoint therapeutics could

have immunological memory responses (Fig. 3c). In agreement with the proposed non-overlapping biological functions of Axl and Mertk, when E0771 Axl KO cells were orthotopically transplanted into Mertk$^{(-/-)}$ mice, tumor growth was additively inhibited (Fig. 3d, S3b,c) and overall tumor-free survival was extended (Fig. 3e), consistent with the idea that TAM receptors contribute multiple independent functions that influence tumor progression on tumor cells and in TME.

To explore molecular mechanisms by which Mertk receptor influences the TME and host anti-tumor immunity, we examined effects of Mertk$^{(-/-)}$ on total macrophage mediated efferocytosis as well as how Mertk knockout effects gene expression patterns following efferocytosis. As shown in Fig. 4a, when bone marrow derived macrophages (BMDMs) were treated with dexamethasone, a known inducer of Mertk expression [15,37–39] both surface expression of Mertk (Fig. 4a) as well as net efferocytosis, measured by increased engulfment of pHrodo^{+} apoptotic cells (ACs), (Fig. 4b) were decreased in the macrophages derived from Mertk$^{(-/-)}$ mice (right panels). Similar results were observed when peritoneal macrophages were co-incubated with pHrodo stained ACs whereby Mertk$^{(-/-)}$ macrophages show decreased efferocytosis (~40%) as compared to Mertk$^{(+/+)}$ macrophages when assessed by either flow cytometry Fig. 4c) or with live time-lapsed microscopic imaging (Fig. 4d).

To assess the most proximal changes in gene expression in an unbiased capacity, we performed RNAseq from wild-type and Mertk$^{(-/-)}$ macrophages following *in vivo* efferocytosis (Fig. 4e). Experimentally, pHrodo stained ACs were injected in to the peritoneal cavity of c57BL/6 Mertk$^{(+/+)}$ and Mertk$^{(-/-)}$ mice for 1 hr, after which peritoneal exudate was recovered and analyzed for CD11b^{+}, F4/80^{+} vs CD11b^{+}, F4/80^{+}, pHrodo^{+} macrophages. While total *in vivo* efferocytosis was decreased approximately 40% in the Mertk deficient mice (Fig. 4f, S4a), for the RNAseq experiments we sorted CD11b^{+}, F4/80^{+} macrophages from untreated mice and CD11b^{+}, F4/80^{+}, pHrodo^{+} macrophages from AC injected mice and normaled the concentration of RNA. Since human cells were used as the source of apoptotic cells, we investigated a potential cross-mapping of human genes as a contamination of RNA. Notably, when the data was mapped to human genome, there was no differences between samples mixed with and without human cells, indicating that human and mouse are sufficiently divergent to be differentiated by mapping using HISAT2 (S4b-c). As indicated in Fig. 4g, Mertk$^{(-/-)}$ macrophages exhibited a general suppression in macrophage activation pathways following efferocytosis, including tuned down inflammatory genes (IL-10, IL-6, CCL4) as well as genes in the biosynthesis of PGE_2 (PTGS2 and Cox-2) compared to WT macrophages (Fig. 4h, S4d). To further validate effects of Mertk on inflammatory cytokine production, 20 ug LPS was injected into the peritoneal cavity to Mertk$^{(+/+)}$ and Mertk$^{(-/-)}$ mice to induce an endotoxin mediated inflammatory response for 4 hrs, after which peritoneal exudate was collected, and assessed for cytokine mRNA using qRT-PCR (Fig. 4i, j). To validate immunosuppressive phenotype of Mertk receptors, Mertk$^{(+/+)}$ and Mertk$^{(-/-)}$ mice were injected 20μg LPS IP, followed by collection of periteonal exudate after 4 hrs (Fig. 4i). The RNA was collected and qRTPCR was performed. Similar to RNASeq analysis, LPS induced immflammatory response was suppressed in Mertk$^{(-/-)}$ mice as compared to Mertk$^{(+/+)}$ mice (Fig. 4j). As compared to PBS treated mice, IL-6 and IL-10 were signficantly increased in the LPS treated Mertk$^{(+/+)}$ mice, however in the Mertk$^{(-/-)}$ mice LPS induced immflammatory response was suppressed. On

the other hand, increased TGF-β expression pattern, but not significant, in the Mertk$^{(+/+)}$ and suppressed TGF-β in Mertk$^{(-/-)}$ mice following LPS treatment was observed. Together, these results suggest that Mertk receptor ablation decreases tumor growth and extends tumor free survival by inhibiting macrophage-dependent efferocytosis and resulting inhibitory pathways regulated by efferocytosis.

Pre-clinical model for Mertk inhibition: Anti-Mertk antibody reduces tumor growth in combination with anti-PD1 immunotherapy.

To extend the aforementioned genetic studies and establish a pre-clinical pharmacological model to suppress Mertk activity *in vitro* and *in vivo,* we employed a novel first in-class anti-Mertk monoclonal antibody (anti-Mertk3), a neutralizing *IgG1* mAb modified to eliminate any potential Fc receptor effector function, that inhibits ligand induced Mertk functions (Fig. 5). When analyzed by cell surface binding analysis, anti-Mertk mAb bound in a dose-dependent manner to mouse Mertk receptor on the peritoneal macrophages (Fig. 5a) and blocked the Mertk mediated engulfment of apoptotic mouse thymocytes when compared to isotype control (Fig. 5b, left panel). By employing surface plasma resonance (SPR) with anti-Mertk3, the equilibrium dissociation constant (KD) for anti-Mertk3 was in the namomolar range (~28 nM) and showed a cell surface EC50 inhibition of 9.8 nM for Gas6-inducible Mertk inhibition (Fig. 5b, right table). To show selectivity of Mertk to Mertk, we used a series of chimeric TAM-IFN-γR1 reporter CHO cells, which fuse the extracellular and trans-membrane domains of murine TAM receptors to the intracellular domain of IFN-γR1 [(40)]. As shown in Fig. 5c, S5a, anti-Mertk3 mAb pre-incubation shows significant dose-dependent blockade of Gas6 and AC-mediated activation of Mertk receptor only, affirming specificity for Mertk and does not cross-react with other TAMs. Subsequently, anti-Mertk mAb was also able to block ligand-mediated Mertk activation when cells were pre-treated with Gas6 prior to addition to anti-Mertk mAb or when Gas6 and anti-Mertk mAb were treated simultaneously (Fig. S5b) showing neutralizing activity in the presence of Gas6 ligand. No changes in receptor internalization was noted with anti-Mertk3, suggesting this antibody mainly has ligand neutraling function(Fig. 5d).

To test the efficacy of anti-Mertk mAb *in vivo,* E0771 WT cells were implanted into the mammary fat pat of c57BL/6 female mice as above, and tumor bearing mice (100 mm^3) were intra-peritoneally administered with either single agents anti-Mertk mAb, anti-PD1 mAb or both in combination (Fig. 5e, S6a,b). Notably, under these conditions the anti-Mertk mAb had no significant single agent effect on tumor growth (Fig. 5e, red versus black), however, when combined with anti-PD1 immunotherapy, anti-Mertk mAb showed enhanced effect on suppression of tumor growth (Fig. 5e) and extended overall survival (Fig. 5f) whereby 6 out of 8 mice were tumor free. In addition, as compared to isotype control, we did not observe any splenomegaly in the mice treated with anti-Mertk and anti-PD1 mAb combination, as indicated by spleen weight (Fig. 5g) and spleen length (Fig. S6c). There was no cytotoxicity of antibody was observed as there was no loss in body weight was recorded (Fig. S6d).

Targeting Axl and Mertk induces distinct tumor infiltrating lymphocytes and promotes tumor immunogenicity.

The above-mentioned studies suggested that, both Axl, intrinsically, and Mertk in the TME may influence tumor growth and modulate immune responses. To further test this idea, we extracted total RNA from snap frozen primary tumors and performed Nanostring pan-cancer immune profiling to examine the frequency of tumor-infiltrating immune cell subsets. We observed that mice treated with anti-Mertk and anti-PD1 mAb combinations showed substantially increased $CD45^+$ lymphocytes (Fig. 6a), total T cells (Fig. 6b), tumor-infiltrating $CD8^+$ cytotoxic T-cells (Fig. 6c). Additionally, neutrophils (Fig. 6d), macrophages (Fig. 6e), and NK cells were also increased in the tumors isolated from the mice treated with anti-Mertk and anti-PD1 mAb combination group as compared to isotype treated mice (Fig. 6f). In contrast, mice bearing Axl KO tumor cells treated with anti-PD1 mAb, showed modest increase in infiltration of $CD8^+$ cytotoxic T-cells as compared to isotype control (Fig. 6c). The mice bearing Axl KO tumor cells or treated with monotherapies, showed baseline expression of these immune cell populations similar to isotype control. These studies, together with results shown in Fig. 3d-e, further suggest that Axl and Mertk impact tumor growth by non-overlapping mechanisms, and also implies that TAMs (i.e. Axl on tumor cells and Mertk on tumor associated monocytes) differentially impact the immune milieu of the TME to induce tumor immunogenicity. In subsequent studies, tumor-free mice following anti-Mertk mAb plus anti-PD1 treatment (6/8 TF) or mice transplanted with Axl KO tumor cells and given anti-PD1 therapy (7/8 TF), were re-challenged with E0771 tumor cells on d42 (0.1×10^6) and d80 (0.2×10^6). Similar to phenotype observed in the $Mertk^{(-/-)}$ mice treated with anti-PD1 therapy (as shown in Fig. 3c), tumors failed to grow in both the treatment groups (Fig. 6g), indicating that targeting Axl and Mertk can suppress tumor growth by promoting host anti-tumor immunity.

T-cell depletion reverses anti-tumor response of Axl KO tumor cells or anti-Mertk mAb treatment in combination with anti-PD1 immunotherapy.

To further explore the effects of a T cell-mediated abscopal effect on the Axl KO tumor bearing versus anti-Mertk mAb treated mice, we replicated tumor growth studies (For Axl KO-Fig. 2g; Anti-Mertk-Fig. 5f) by depleting cytotoxic $CD8^+$ T-cells. To deplete $CD8^+$ T-cells mice were injected intraperitoneally 200 μg anti-CD8α mAb, a day before tumor cell injection and was repeated every 3 days until the end of the study (Fig. S6e). Consistent with T cell responses being necessary for effective anti-tumor immune responses, under the conditions of $CD8^+$ T-cell depletion, the observed efficacies of Axl KO alone and with anti-PD1 therapeutics were only partially reversed, (Fig. 7a Left panel, b) whereas, anti-tumor efficacy of anti-Mertk mAb in combination with anti-PD1 therapeutics was completely inhibited (Fig. 7a Middle panel, b). The reducation in the tumor growth among anti-CD8α mAb non-treated and treated treatment groups were provided as a table for comparison (Fig. 7a Right table). Similarly, when we performed these studies in B6.CB17-Prkdc SCID mice, which lack functional T and B cells (Fig. 7c), tumor growth of Axl KO cells was reduced, whereas no changes in the tumor growth in the mice treated with anti-Mertk mAb was observed as compared to isotype treated mice (Fig. 7c, S6f). The mice injected with Axl KO tumor cells or administered anti-Mertk mAb, showed similar percentage tumor free survival as compared to isotype control (Fig. 7d). Taken together, these data suggest that both Axl,

primarily affecting tumorigenic properties of the tumor cells and Mertk, via macrophage efferocytosis modulating immune cell infiltration within the TME towards inflamed tumor milieu in a E0771 breast cancer model.

Discussion

Over the past several years TAM receptors have emerged as an important class of oncogenic receptors that have roles in oncology and immune-oncology [8,9]. When overexpressed or dysregulated on tumor cells, TAMs can drive tumor progression by acting directly as oncogenic tyrosine kinases [41], but recent data also indicates TAMs, particularly Mertk, function as immune inhibitory receptors expressed on myeloid-derived cells that comprise the local and systemic host TME. Here, we explored this arrangement of TAM receptors in an immunotherapy cancer model using triple negative breast cancer models whereby Axl is predominantly expressed on tumor cells, while Mertk is expressed on immune cells in the TME. We show that both of the aforementioned signals contribute to overall tumorigenicity and metastasis, and interestingly, both pathways when inhibited synergize with anti-PD1 mAb therapeutics and shows improved pre-clinical outcomes. Collectively, our data suggest that TAMs contribute multiple overlapping signaling events, including both cell intrinsic and cell extrinsic to promote progression. Indeed, loss of Axl function in E0771 cells also synergized when transplanted into Mertk$^{(-/-)}$ mice, demonstrating that TAMs in different subcellular compartments crosstalk to alter tumor outcomes and host anti-tumor immune responses. Our results suggest that specific combinations of individual TAM inhibitors may be employed to decrease tumor progression and activate host immunity in the complex tumor microenvironment.

Our present approach, using both a genetic knockout strategy and a neutralizing anti-Mertk mAb, showed that inhibition of Mertk in the tumor microenvironment also promotes a host anti-tumor response, particularly in combination with anti-PD1 immunotherapy. While the mechanisms by which Mertk acts as an inhibitory receptor are likely to be multi-factorial and complex, our present data indicates an important function for Mertk is control macrophage efferocytosis and resulting changes in gene expression associated with efferocytosis, including inhibitory cytokines, chemokines, and genes associated with PGE_2 production. Recent studies by Zhou et al have shown that blockage of Mertk functionally synergizes with anti-PD1 mAb in MC38 and E0771 tumor models and functions via a type I IFN-β driven by cGAS/Sting [25]. While we did not observe the up-regulation of IFN-stimuted genes (ISG) in the Mertk (−/−) macrophages by RNAseq at early times (1 hr post-efferocytosis), it is possible that IFN-dependent signatures are induced at later times in the TME, or are induced by different subsets of macrophages such as tumor associated macrophages.

Our studies also indicate that inhibition of Mertk in the TME ultimately results in the development and maintenance of a T-cell mediated abscopal effect, supported by several independent experiments that include (i) mice are protected from subsequent tumor growth by re-challenge in a different flank, (ii) protective effects are abrogated by depletion of $CD8^+$ T-cells using anti-CD8α mAb, (iii) anti-Mertk mAb is less effective in B6-SCID mice that lack T cells, and (iv) Nanostring profiling showing a significant infiltration of

cytotoxic CD8+ T cells into the tumor. While a recent study showed that Mertk expressed on T cells, could function as a co-stimulatory receptor to enhance TCR signaling and antigen-dependent cell killing, it is possible that the inhibitory signals on macrophages and other myeloid cells represent a more dominant signaling for inducing anti-tumor effects of Mertk therapeutics. Collectively, our present data show that targeting Mertk in the TME can effectively potentiate a T cell-mediated anti-tumor host response in the E0771 breast cancer model.

As macrophages particularly the tumor-associated M2 macrophages, are the principle cell type that express Mertk [34,38,42,43], one attractive mechanistic possibility is that the inhibition of Mertk not only blocks the immune suppressing effects of macrophage efferocytosis as alluded to above, but permits preferential efferocytosis into cross presenting dendritic cells (DCs), for example in cells that express higher levels of Axl and do not depend on Mertk for efferocytosis. Such an “efferocytosis shunt” mechanism would be expected to permit uptake and processing of tumor antigens into DCs (a cross presentation competent cell type), but restrict suppressive cytokines produced by macrophages that prevent migration and maturation of DCs to the draining lymph nodes where cross-presentation and activation of tumor-specific cytotoxic T-lymphocytes is achieved (Fig. 7e). Such a mechanism to alter the cell type by which efferocytosis occurs is envisioned to be mechanistically distinct to anti-CD47 therapeutics, that reverse don’t eat me signals and favor increased net engulfment of live cells [44–46].

While these data collectively point to an immune inhibitory role for Mertk in the E0771 model developed in this study and is consistent with previous studies by Cook and colleagues [22] and Brekken and colleagues [47,48] that employed tolerogenic breast and lung cancer models, we are also cognizant that inhibiting Mertk or Axl in tumors driven by inflammatory pathways may not benefit from inhibition of TAMs. For example, studies by Rothlin and colleagues, employing a DSS inflammatory model of colon cancer [49], showed that Mertk and Axl double knockout promoted more aggressive tumor growth than WT mice, contrary to the results observed in our study. Moreover, studies by Tavazoie and colleagues [50] showed that agonistic Mertk antibodies blocked circulating endothelial cell recruitment into tumors, and presently it is unclear whether Mertk inhibitory antibodies might impact tumor angiogenesis in certain tumors.

Collectively, the studies here indicate that TAMs have both distinct and overlapping functions in the TME, with notable crosstalk between receptors expressed on different cell types. The studies also suggest that different TAM targeting strategies (pan-TAM, versus anti-Mertk, versus anti-Axl) will be empirically determined by the expression of TAMs on the tumor cells and should be segregated by Axl positive versus Axl negative expression. Finally, these studies are consistent with a growing body of evidence that targeting Mertk, akin to a myeloid checkpoint inhibitor, should be further explored as an attractive anti-cancer therapeutic modality in combination with other checkpoint and immune-oncology applications.

Supplementary Material

Refer to Web version on PubMed Central for supplementary material.

Acknowledgments

We thank Sukhwinder Singh of Rutgers University Flow cytometry core facility for flow cytometry technical support and cell sorting. We thank NYU genomic core facility for NanoString analysis and technical support. We also thank Dr. Edward Thorp (Northwestern) for providing the Mertk knockout mice.

References

1. Farkona S, Diamandis EP, Blasutig IM. Cancer immunotherapy: the beginning of the end of cancer? BMC Med 2016;14:73 [PubMed: 27151159]
2. Sharma P, Allison JP. Immune checkpoint targeting in cancer therapy: toward combination strategies with curative potential. Cell 2015;161:205–14 [PubMed: 25860605]
3. Birge RB, Boeltz S, Kumar S, Carlson J, Wanderley J, Calianese D, et al. Phosphatidylserine is a global immunosuppressive signal in efferocytosis, infectious disease, and cancer. Cell Death Differ 2016;23:962–78 [PubMed: 26915293]
4. Dayoub AS, Brekken RA. TIMs, TAMs, and PS- antibody targeting: implications for cancer immunotherapy. Cell Commun Signal 2020;18:29 [PubMed: 32087708]
5. Cheng X, Li L, Thorpe PE, Yopp AC, Brekken RA, Huang X. Antibody-Mediated Blockade of Phosphatidylserine Enhances the Antitumor Effect of Sorafenib in Hepatocellular Carcinomas Xenografts. Ann Surg Oncol 2016;23:583–91 [PubMed: 26847681]
6. Ran S, Thorpe PE. Phosphatidylserine is a marker of tumor vasculature and a potential target for cancer imaging and therapy. Int J Radiat Oncol Biol Phys 2002;54:1479–84 [PubMed: 12459374]
7. Graham DK, DeRyckere D, Davies KD, Earp HS. The TAM family: phosphatidylserine sensing receptor tyrosine kinases gone awry in cancer. Nat Rev Cancer 2014;14:769–85 [PubMed: 25568918]
8. Akalu YT, Rothlin CV, Ghosh S. TAM receptor tyrosine kinases as emerging targets of innate immune checkpoint blockade for cancer therapy. Immunol Rev 2017;276:165–77 [PubMed: 28258690]
9. Rothlin CV, Carrera-Silva EA, Bosurgi L, Ghosh S. TAM receptor signaling in immune homeostasis. Annu Rev Immunol 2015;33:355–91 [PubMed: 25594431]
10. Nagata K, Ohashi K, Nakano T, Arita H, Zong C, Hanafusa H, et al. Identification of the product of growth arrest-specific gene 6 as a common ligand for Axl, Sky, and Mer receptor tyrosine kinases. J Biol Chem 1996;271:30022–7 [PubMed: 8939948]
11. Anderson HA, Maylock CA, Williams JA, Paweletz CP, Shu H, Shacter E. Serum-derived protein S binds to phosphatidylserine and stimulates the phagocytosis of apoptotic cells. Nature immunology 2003;4:87–91 [PubMed: 12447359]
12. Lee YJ, Han JY, Byun J, Park HJ, Park EM, Chong YH, et al. Inhibiting Mer receptor tyrosine kinase suppresses STAT1, SOCS1/3, and NF-kappaB activation and enhances inflammatory responses in lipopolysaccharide-induced acute lung injury. Journal of leukocyte biology 2012;91:921–32 [PubMed: 22427680]
13. Camenisch TD, Koller BH, Earp HS, Matsushima GK. A novel receptor tyrosine kinase, Mer, inhibits TNF-alpha production and lipopolysaccharide-induced endotoxic shock. J Immunol 1999;162:3498–503 [PubMed: 10092806]
14. Zhang B, Lu H, Jiang A, Wu H, Fang L, Lv Y. MerTK Downregulates Lipopolysaccharide-Induced Inflammation Through SOCS1 Protein but Does Not Affect Phagocytosis of Escherichia coli in Macrophages. Inflammation 2019;42:113–23 [PubMed: 30143932]
15. Zizzo G, Cohen PL. The PPAR-gamma antagonist GW9662 elicits differentiation of M2c-like cells and upregulation of the MerTK/Gas6 axis: a key role for PPAR-gamma in human macrophage polarization. J Inflamm (Lond) 2015;12:36 [PubMed: 25972766]

16. Fadok VA, Bratton DL, Konowal A, Freed PW, Westcott JY, Henson PM. Macrophages that have ingested apoptotic cells in vitro inhibit proinflammatory cytokine production through autocrine/paracrine mechanisms involving TGF-beta, PGE2, and PAF. J Clin Invest 1998;101:890–8 [PubMed: 9466984]
17. Munoz LE, Lauber K, Schiller M, Manfredi AA, Herrmann M. The role of defective clearance of apoptotic cells in systemic autoimmunity. Nature reviews Rheumatology 2010;6:280–9 [PubMed: 20431553]
18. Behrens EM, Gadue P, Gong SY, Garrett S, Stein PL, Cohen PL. The mer receptor tyrosine kinase: expression and function suggest a role in innate immunity. Eur J Immunol 2003;33:2160–7 [PubMed: 12884290]
19. Lu Q, Lemke G. Homeostatic regulation of the immune system by receptor tyrosine kinases of the Tyro 3 family. Science 2001;293:306–11 [PubMed: 11452127]
20. Thorp E, Cui D, Schrijvers DM, Kuriakose G, Tabas I. Mertk receptor mutation reduces efferocytosis efficiency and promotes apoptotic cell accumulation and plaque necrosis in atherosclerotic lesions of apoe−/− mice. Arterioscler Thromb Vasc Biol 2008;28:1421–8 [PubMed: 18451332]
21. Petta S, Valenti L, Marra F, Grimaudo S, Tripodo C, Bugianesi E, et al. MERTK rs4374383 polymorphism affects the severity of fibrosis in non-alcoholic fatty liver disease. J Hepatol 2016;64:682–90 [PubMed: 26596542]
22. Cook RS, Jacobsen KM, Wofford AM, DeRyckere D, Stanford J, Prieto AL, et al. MerTK inhibition in tumor leukocytes decreases tumor growth and metastasis. J Clin Invest 2013;123:3231–42 [PubMed: 23867499]
23. Crittenden MR, Baird J, Friedman D, Savage T, Uhde L, Alice A, et al. Mertk on tumor macrophages is a therapeutic target to prevent tumor recurrence following radiation therapy. Oncotarget 2016;7:78653–66 [PubMed: 27602953]
24. Tormoen GW, Blair TC, Bambina S, Kramer G, Baird J, Rahmani R, et al. Targeting MerTK Enhances Adaptive Immune Responses After Radiation Therapy. Int J Radiat Oncol Biol Phys 2020;108:93–103 [PubMed: 32311417]
25. Zhou Y, Fei M, Zhang G, Liang WC, Lin W, Wu Y, et al. Blockade of the Phagocytic Receptor MerTK on Tumor-Associated Macrophages Enhances P2X7R-Dependent STING Activation by Tumor-Derived cGAMP. Immunity 2020;52:357–73 e9 [PubMed: 32049051]
26. Asiedu MK, Beauchamp-Perez FD, Ingle JN, Behrens MD, Radisky DC, Knutson KL. AXL induces epithelial-to-mesenchymal transition and regulates the function of breast cancer stem cells. Oncogene 2014;33:1316–24 [PubMed: 23474758]
27. Gjerdrum C, Tiron C, Hoiby T, Stefansson I, Haugen H, Sandal T, et al. Axl is an essential epithelial-to-mesenchymal transition-induced regulator of breast cancer metastasis and patient survival. Proc Natl Acad Sci U S A 2010;107:1124–9 [PubMed: 20080645]
28. Goyette MA, Duhamel S, Aubert L, Pelletier A, Savage P, Thibault MP, et al. The Receptor Tyrosine Kinase AXL Is Required at Multiple Steps of the Metastatic Cascade during HER2-Positive Breast Cancer Progression. Cell Rep 2018;23:1476–90 [PubMed: 29719259]
29. Hardy SD, Shinde A, Wang WH, Wendt MK, Geahlen RL. Regulation of epithelial-mesenchymal transition and metastasis by TGF-beta, P-bodies, and autophagy. Oncotarget 2017;8:103302–14 [PubMed: 29262563]
30. Shinde A, Hardy SD, Kim D, Akhand SS, Jolly MK, Wang WH, et al. Spleen Tyrosine Kinase-Mediated Autophagy Is Required for Epithelial-Mesenchymal Plasticity and Metastasis in Breast Cancer. Cancer Res 2019;79:1831–43 [PubMed: 30733195]
31. Colavito SA. AXL as a Target in Breast Cancer Therapy. J Oncol 2020;2020:5291952 [PubMed: 32148495]
32. Leconet W, Chentouf M, du Manoir S, Chevalier C, Sirvent A, Ait-Arsa I, et al. Therapeutic Activity of Anti-AXL Antibody against Triple-Negative Breast Cancer Patient-Derived Xenografts and Metastasis. Clin Cancer Res 2017;23:2806–16 [PubMed: 27923843]
33. Kasikara C, Kumar S, Kimani S, Tsou WI, Geng K, Davra V, et al. Phosphatidylserine Sensing by TAM Receptors Regulates AKT-dependent Chemoresistance and PD-L1 Expression. Molecular cancer research : MCR 2017

34. Kasikara C, Davra V, Calianese D, Geng K, Spires TE, Quigley M, et al. Pan-TAM Tyrosine Kinase Inhibitor BMS-777607 Enhances Anti-PD-1 mAb Efficacy in a Murine Model of Triple-Negative Breast Cancer. Cancer Res 2019;79:2669–83 [PubMed: 30877108]
35. Moynihan KD, Opel CF, Szeto GL, Tzeng A, Zhu EF, Engreitz JM, et al. Eradication of large established tumors in mice by combination immunotherapy that engages innate and adaptive immune responses. Nat Med 2016;22:1402–10 [PubMed: 27775706]
36. Aslakson CJ, Miller FR. Selective events in the metastatic process defined by analysis of the sequential dissemination of subpopulations of a mouse mammary tumor. Cancer Res 1992;52:1399–405 [PubMed: 1540948]
37. Scott RS, McMahon EJ, Pop SM, Reap EA, Caricchio R, Cohen PL, et al. Phagocytosis and clearance of apoptotic cells is mediated by MER. Nature 2001;411:207–11 [PubMed: 11346799]
38. Zagorska A, Traves PG, Lew ED, Dransfield I, Lemke G. Diversification of TAM receptor tyrosine kinase function. Nat Immunol 2014;15:920–8 [PubMed: 25194421]
39. Zahuczky G, Kristof E, Majai G, Fesus L. Differentiation and glucocorticoid regulated apopto-phagocytic gene expression patterns in human macrophages. Role of Mertk in enhanced phagocytosis. PloS one 2011;6:e21349 [PubMed: 21731712]
40. Tsou WI, Nguyen KQ, Calarese DA, Garforth SJ, Antes AL, Smirnov SV, et al. Receptor tyrosine kinases, TYRO3, AXL, and MER, demonstrate distinct patterns and complex regulation of ligand-induced activation. J Biol Chem 2014;289:25750–63 [PubMed: 25074926]
41. Huey MG, Minson KA, Earp HS, DeRyckere D, Graham DK. Targeting the TAM Receptors in Leukemia. Cancers (Basel) 2016;8
42. Nishi C, Toda S, Segawa K, Nagata S. Tim4- and MerTK-mediated engulfment of apoptotic cells by mouse resident peritoneal macrophages. Mol Cell Biol 2014;34:1512–20 [PubMed: 24515440]
43. Zizzo G, Hilliard BA, Monestier M, Cohen PL. Efficient clearance of early apoptotic cells by human macrophages requires M2c polarization and MerTK induction. J Immunol 2012;189:3508–20 [PubMed: 22942426]
44. Barclay AN, Van den Berg TK. The interaction between signal regulatory protein alpha (SIRPalpha) and CD47: structure, function, and therapeutic target. Annual review of immunology 2014;32:25–50
45. Jaiswal S, Jamieson CH, Pang WW, Park CY, Chao MP, Majeti R, et al. CD47 is upregulated on circulating hematopoietic stem cells and leukemia cells to avoid phagocytosis. Cell 2009;138:271–85 [PubMed: 19632178]
46. Zhang M, Hutter G, Kahn SA, Azad TD, Gholamin S, Xu CY, et al. Anti-CD47 Treatment Stimulates Phagocytosis of Glioblastoma by M1 and M2 Polarized Macrophages and Promotes M1 Polarized Macrophages In Vivo. PloS one 2016;11:e0153550 [PubMed: 27092773]
47. Du W, Huang H, Sorrelle N, Brekken RA. Sitravatinib potentiates immune checkpoint blockade in refractory cancer models. JCI Insight 2018;3
48. Kirane A, Ludwig KF, Sorrelle N, Haaland G, Sandal T, Ranaweera R, et al. Warfarin Blocks Gas6-Mediated Axl Activation Required for Pancreatic Cancer Epithelial Plasticity and Metastasis. Cancer research 2015;75:3699–705 [PubMed: 26206560]
49. Bosurgi L, Bernink JH, Delgado Cuevas V, Gagliani N, Joannas L, Schmid ET, et al. Paradoxical role of the proto-oncogene Axl and Mer receptor tyrosine kinases in colon cancer. Proc Natl Acad Sci U S A 2013;110:13091–6 [PubMed: 23878224]
50. Png KJ, Halberg N, Yoshida M, Tavazoie SF. A microRNA regulon that mediates endothelial recruitment and metastasis by cancer cells. Nature 2012;481:190–4

Significance:

This study demonstrates how TAM receptoprs act both as oncogenic tyrosine kinases and as receptors that mediate immune evasion in cancer progression.

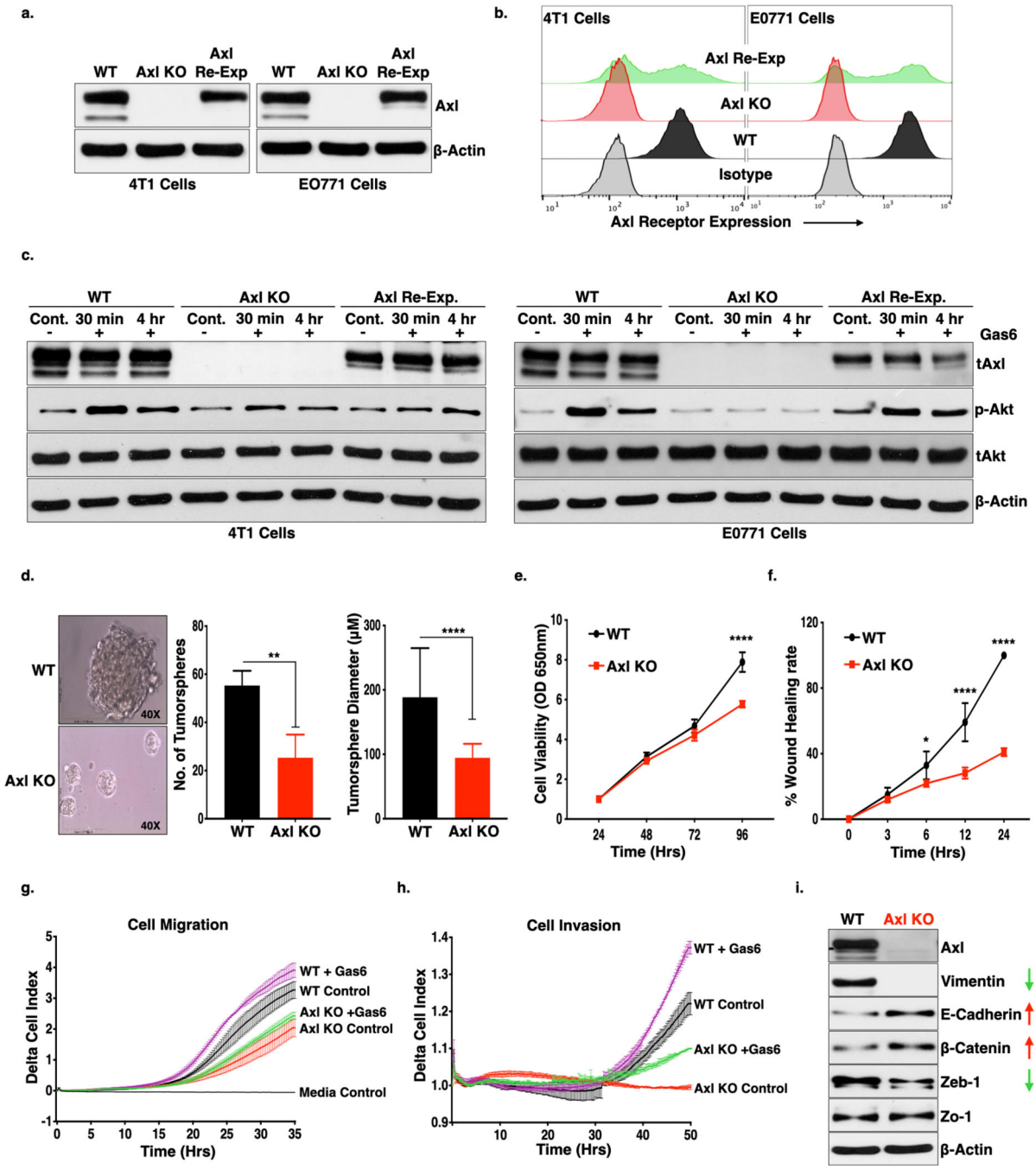

Figure 1. Genetic deletion of Axl receptor in murine breast cancer cells inhibit cell proliferation, formation of tumorspheres, cell motility and tumor growth in the preclinical murine breast cancer model.

(a-b.) Western blot **(a.)** and flow cytometry **(b.)** analysis of Axl receptor knockout (KO) using CRISPR/Cas9 technology and retroviral re-expression of Axl receptor in the Axl KO cells in the triple-negative (ER, PR or Her2/Neu) murine breast cancer 4T1-Luc-GFP and E0771 cells. **c.** Ligand, Gas6, mediated activation of Axl receptor was analyzed as phosphorylation of Akt (downstream signaling molecule of Axl) following Gas6 treatment for 30 mins and 4 hrs., in the 4T1 and E0771- WT, Axl KO and Axl Re-Exp. cells

by immunoblot analysis. **d.** Tumorsphere formation from 4T1-WT and Axl KO cells on the ultra-low attachment plate. Phase-contrast micrographs representing tumorspheres (left panel) and column graphs showing number and size of tumorspheres formed from 1000–4T1- WT and Axl KO cells. **P<0.01, ****P<0.001. Mean values ± SD are shown (n = 12). **e.** The effect of Axl receptor KO on cell proliferation as compared to 4T1-WT as analyzed MTT assay for 4 days. Mean values ± SD are shown (n = 8). **f.** Cell migration of the 4T1-WT and Axl KO as determined by wound healing assay. **g-h.** Real time cell migration **(f)** and invasion **(g)** of the 4T1-WT and Axl KO cells in the presence or absence of Gas6 through microporous membrane of CIM plates using Real-time xCELLigence system. Difference in the rate of migration and invasion was analyzed by two-way ANOVA. **i.** Axl deletion induces loss of mesenchymal markers, Vimentin and Zeb-1 and increase in epithelial markers, E-Cadherin and β-Catenin expression as analyzed by Western blot analysis of protein lysates from 4T1-WT and Axl KO cells.

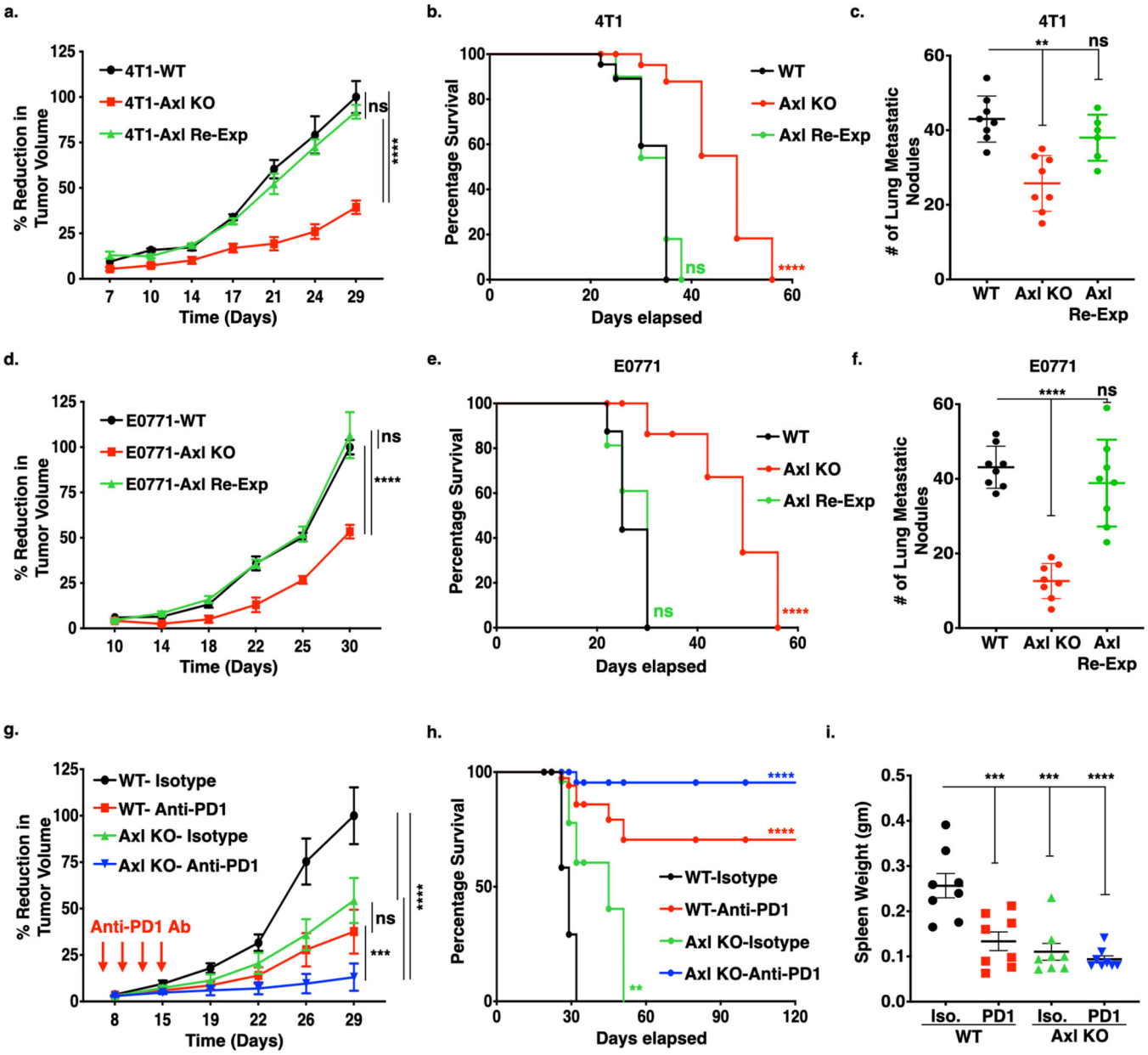

Figure 2. Genetic Ablation of Axl receptor alone or in combination with anti-PD1 immunotherapy impairs tumor growth and metastasis in the murine breast cancer models.

(a-f.) *In vivo* tumor growth curves, corresponding Kaplan-Meier curves and number of lung metastatic nodules of 4T1 and E0771 tumor models. 5 X 10^4 4T1- **(a.)** and E0771-WT, Axl KO and Axl Re-Exp. **(d.)** cells were injected orthotopically into the mammary fat pad of 8-weeks BALB/c and c57BL/6 female mice respectively and tumor growth determined by means tumor volume measurement every 3 days over the period of 5 weeks. Kaplan-Meier curves depicting percentage survival of tumor bearing mice in corresponding 4T1 **(b.)** and E0771 **(e.)** tumors. Quantification of microscopic lung metastatic nodules from 4T1 **(c.)** and E0771 **(f.)** tumor bearing mice following lungs harvests at sacrifice on d35 and fixation bouin solution. **g.** Tumor growth analysis of E0771-WT and Axl KO tumor bearing mice

(n=8/group) treated with mIgG1 Isotype control Ab or anti-PD1 Ab (5 mg/kg) on day 6, 9, 12, and 15. Arrows indicate antibody injections. **h.** Kaplan-Meier curve showing percentage survival of tumor bearing mice upon anti-PD1 immunotherapy. **i.** Analysis of splenomegaly, as a measure of extramedullary hematopoiesis, in the treated mice by means of spleen weight at sacrifice on d35. *P<0.05, ****P<0.001. Mean values ± SD are shown ($n = 8$).

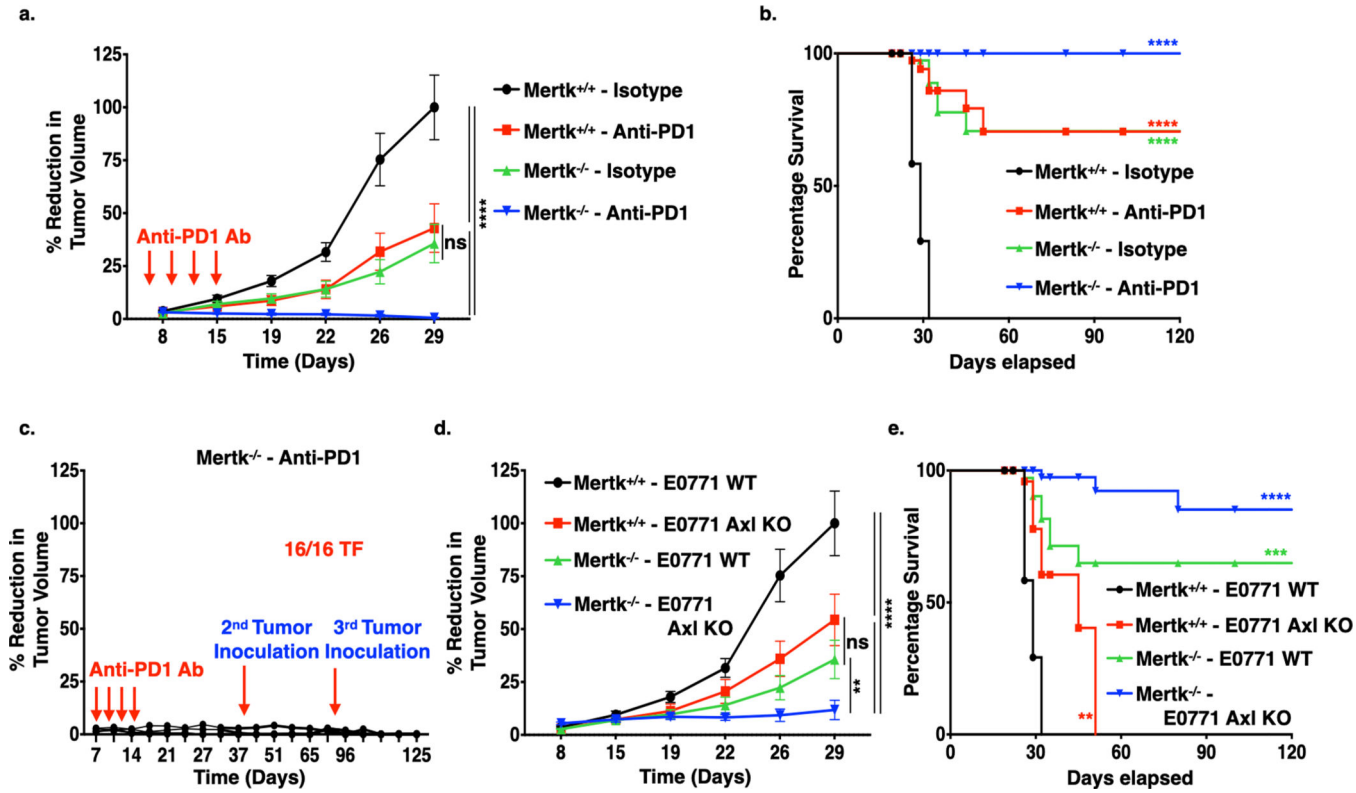

Figure 3. Mertk deficiency decreases tumor malignancy and synergize with anti-PD1 immunotherapy in the E0771 murine breast cancer model.

a. 5X10^4 E0771 WT cells were injected orthotopically in to the mammary fat pad of female c57BL/6- Mertk$^{+/+}$ (WT) and Mertk$^{-/-}$ (Mertk KO) mice, and upon establishment of tumors, mice were treated with mIgG1 Isotype or anti-PD1 antibody (5 mg/kg) on day 6, 9, 12, and 15 and tumor growth determined by means tumor volume measurement every 3 days over the period of 5 weeks. (n=8/per group). Arrows indicate antibody injections. **b.** Kaplan-Meier curve showing percentage survival of tumor bearing mice upon anti-PD1 immunotherapy in the Mertk$^{+/+}$ and Mertk$^{-/-}$ mice. **c.** Tumor free Mertk$^{-/-}$ mice treated with anti-PD1 immunotherapy were rechallenged with 1 X 10^5 or 2 X 10^5 E0771 WT cells d42 and d82 respectively, and tumor growth measurements were performed (n=16). **d-e.** Tumor growth curve **(d.)** and corresponding Kaplan-Meier curves **(e.)** showing percentage survival following injection of 5X10^4 E0771 WT or Axl KO tumor cells in to the mammary fat pad of female c57BL/6- Mertk$^{+/+}$ and Mertk$^{-/-}$ mice.

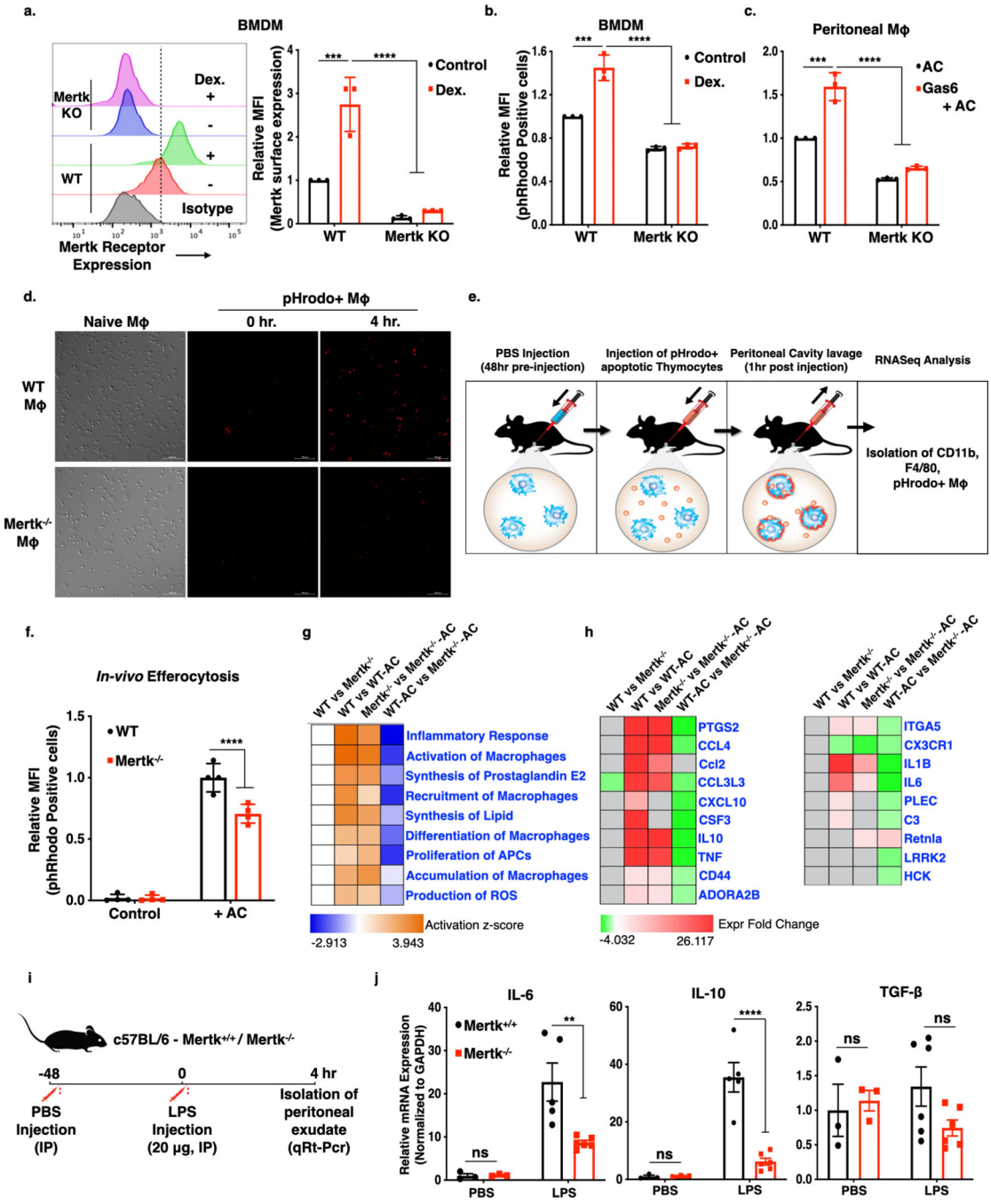

Figure 4. Mertk$^{(-/-)}$ macrophages decreases apoptotic cell efferocytosis and suppression of cytokine production in response to intraperitoneal LPS injection.

a. Mertk receptor expression in BMDM cultures upon stimulation with 0.1μM dexamethasone for 24 hrs. **b.** Flow cytometry analysis of efferocytosis in the dexamethasone treated Mertk$^{(+/+)}$ (WT) and Mertk$^{(-/-)}$ BMDMs. The efferocytosis was quantified by analyzing phRhodo positive macrophages after engulfment of stained irradiated CEM cells. The bar graphs showing normalized phRodo positive cells by mean fluorescence intensity. **c.** Peritoneal macrophages from Mertk$^{(-/-)}$ mice display decreased efferocytosis of phRodo

stained irradiated CEM cells as compared to macrophages isolated from Mertk$^{(+/+)}$ mice. **d.** Efferocytosis in Mertk$^{(+/+)}$ and Mertk$^{(-/-)}$ peritoneal macrophages as analyzed by live imaging over the 4 hrs. **e, f.** Experimental mouse model depicting *in vivo* efferocytosis, where phRodo stained irradiated CEM cells injected in the peritoneal cavity of the mice for 1 hr, following by analysis for CD11b F4/80 positive macrophages with engulfed apoptotic cells. g. RNAseq analysis depicting signaling pathways affected by efferocytosis of apoptotic cells, when analzed by ingenuity pathway analysis. h. Gene expression analysis for genes modulated in inflammatory response and activation of macrophages pathways. **i.** The outline of LPS treatment in the c57BL/6- Mertk$^{(+/+)}$ and Mertk$^{(-/-)}$ mice. **j.** Mice were primed with 1 ml PBS injection into the peritoneal cavity. After 48 hrs, 20 μg LPS was injected intraperitoneally for 4 hrs, followed by isolation of peritoneal exudate, RNA isolation and qRT-PCR for cytokines including IL-6, IL-10 and TGF-β.

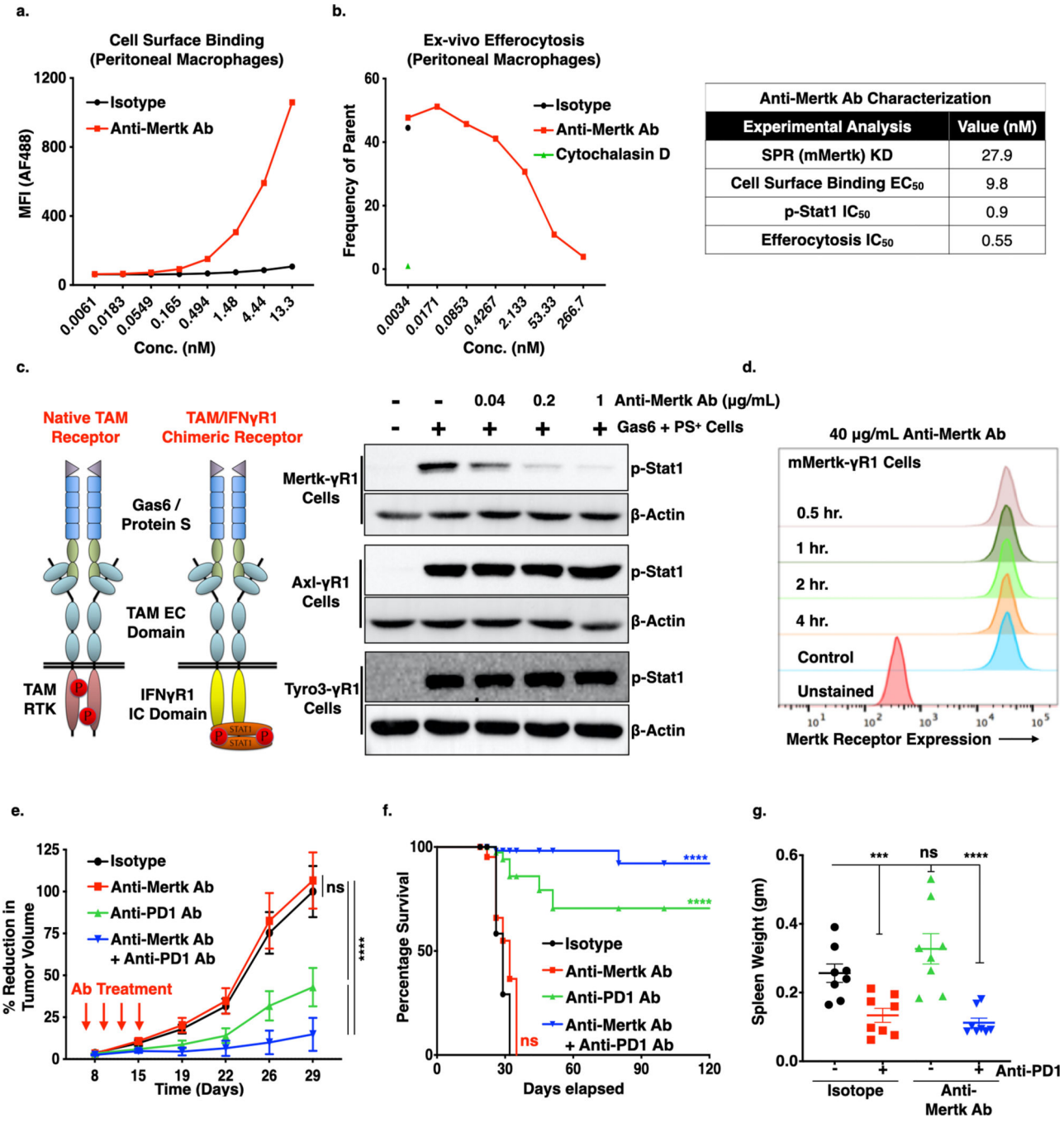

Figure 5. Effect of Anti-Mertk antibody on the Mertk receptor inhibition, efferocytosis, tumor growth and metastasis.

a. Cell surface binding analysis of Anti-Mertk monoclonal antibody (mAb) to the Mertk receptor on the peritoneal macrophages. **b.** *In vivo* efferocytosis showing decreased engulfment of apoptotic mouse thymocytes in the presence of anti-Mertk mAb as compared to isotype control. Cytochalasin D was used as a positive control **(Left panel)**. Characterization of anti-Mertk antibody by surface plasma resonance (SPR) binding analysis, cell surface binding, p-Stat1 activation analysis in chimeric murine Mertk-γR1

cells and in vivo efferocytosis **(Right tabel)**. **d.** Immunoblot analysis showing anti-Mertk antibody induced inhibition of Gas6 and apoptotic cells mediated activation Tyro3, Axl and Mertk receptors in the CHO cells expressing chimeric murine TAM-γR1 receptors. **e.** Flow-Cytometry based analysis showing effect of 40 μg/ml anti-Mertk ab on the Mertk receptor internalization in the CHO murine Mer-γR1 chimeric cells over the period of 4 hrs using Mertk specific flow-based antibody. **f.** Anti-tumor effect of anti-Mertk mAb in combination with Anti-PD1 immunotherapy. E0771 tumor bearing females C57/B16 (n=8/per group) were treated with mIgG1 Isotype control, anti-Mertk aAb (10mg/kg), anti-PD1 ab (5mg/Kg) alone and anti-Mertk ab in combination with anti-PD1 ab on day 6, 9,12, and15 and tumor growth was studied twice a week over the period of 4 weeks. **g.** Kaplan-Meier curve showing percentage survival of tumor bearing mice upon treatment with anti-Mertk ab and anti-PD1 immunotherapy. **h.** Upon sacrifice, spleens were also collected, and splenomegaly was quantified by means of spleen weight. *P<0.05, ****P<0.001. Mean values ± SD are shown ($n = 8$).

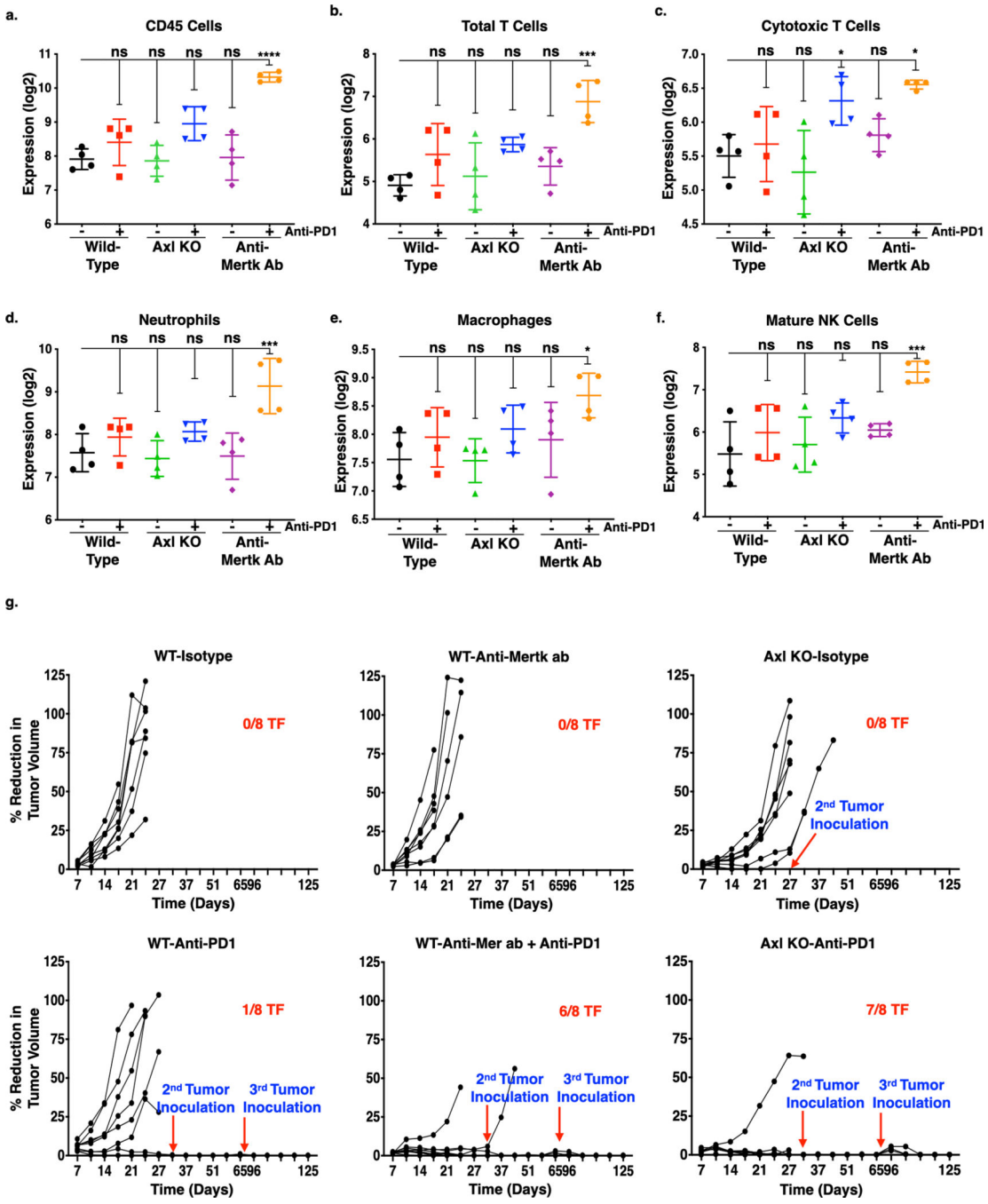

Figure 6. Effect of Axl receptor KO and anti-Mertk ab alone or in combination with anti-PD1 immunotherapy on innate immune cell infiltration and memory T-cell response in the primary mouse breast tumor.

The NanoString nCounter PanCancer immune profiling panel consisting of 770 genes for 24 different immune cell types and population characterization was uses to analyze immune cell infiltration in the primary tumors from each group (n = 4). **a-g.** The cell-type score comparison on the infiltrated immune cells in the primary tumors from each group were presented in log2 and graphically represented by GraphPad Prism. Expression profile of CD45 cells (CD45) **(a)**, total T-cells (CD3D, CD3E, CD3G, CD6, SH2D1A) **(b)**, cytotoxic

T-cells (CD8A, CD8B, GZMA, GZMB, CD94, PRF1) **(c)**, neutrophils (CSF3R, CD16, S100A12) **(d)**, macrophages (CD163, CD68, CD84) **(e)**, and mature NK (CD56dim) cells (NKp46, IL21R, KIR2DL3, KIR3DL1) **(f)**. *P<0.05, **P<0.01, ****P<0.001. Mean values ± SD are shown (n = 4). **g.** Tumor free mice from E0771 WT and Axl KO tumor bearing mice treated with or without anti-PD1 mAb or E0771 WT tumor bearing mice treated with anti-Mertk mAb with or without anti-PD1 immunotherapy were rechallenged with 1 X 10^5 or 2 X 10^5 E0771 WT cells d42 and d82 respectively, and tumor growth measurements were performed up to d120 (n=8).

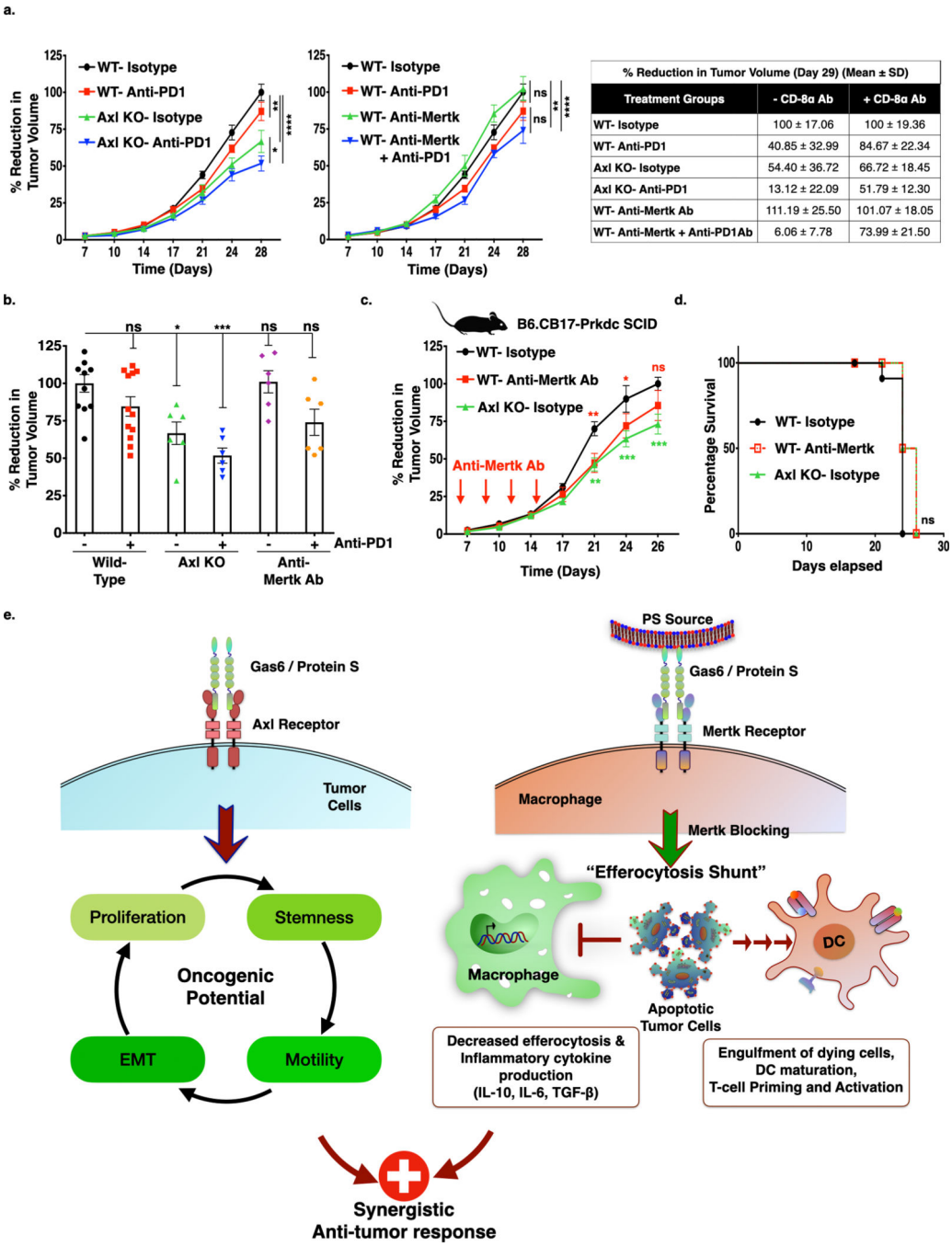

Figure 7. Anti-tumor effect of Axl receptor KO and anti-Mertk Antibody alone or in combination with anti-PD1 immunotherapy is T-cell dependent.

a. The Anti-CD8α antibody, which blocks CD8+ T-cell mediated immune response, has partially blocked anti-tumor effect of Axl receptor KO **(Left panel)**, whereas completely blocked the anti-Mertk ab **(Middle panel)** mediated response in the combination with anti-PD1 immunotherapy. Comparision of decrease in tumor growth between mice treated with or without Anti-CD8α antibody at day 29. **(Right table). b.** Bar graph representing tumor growth at d28 from the individual mice from each group treated with Anti-CD8α antibody.

(n=6–12) **c.** Graph representing tumor growth of Axl KO cells or WT tumor cells or WT tumor bearing mice treated with anti-Mertk antibody in the B6.CB17-Prkdc SCID mice. (n=6). **d.** Kaplan-Meier curve showing percentage survival in the SCID mice. **e.** Dual roles for Axl and Mertk contribute to tumorigenesis by distinct mechanisms. Axl, the expressed mainly on E0771 and 4T1 tumor cells, drives aggressive hallmarks of tumors by affecting stemness, migration, invasion, and EMT. Mertk, on the other hand, effects immunogenic signals in the TME, including efferocytosis and production of cytokines that impinge on the tumor milieu. We propose that anti-Mertk mAbs may block macrophage efferocytosis and the associated immunosuppressive effects associated with M2 macrophage activities.